

Fe $K\alpha$ line emission from the Arches cluster region – evidence for ongoing particle bombardment?

R. Capelli¹, R. S. Warwick², D. Porquet³, S. Gillessen¹, and P. Predehl¹

¹ Max-Planck-Institut für Extraterrestrische Physik, Giessenbachstrasse 1, 85748 Garching, Germany
e-mail: capelli@mpe.mpg.de

² Department of Physics and Astronomy, University of Leicester, Leicester LE1 7RH, UK

³ Observatoire Astronomique de Strasbourg, Université de Strasbourg, CNRS, UMR 7550, 11 rue de l'Université, 67000 Strasbourg, France

Received 25 January 2011 / Accepted 25 March 2011

ABSTRACT

Context. Bright Fe- $K\alpha$ line emission at 6.4 keV is a unique characteristic of some of the dense molecular complexes present in the Galactic center region. Whether this X-ray fluorescence is due largely to the irradiation of the clouds by X-ray photons or is, at least in part, the result of cosmic-ray particle bombardment, remains an interesting open question.

Aims. We present the results of *XMM-Newton* observations performed over the last eight years of the region surrounding the Arches cluster in the Galactic center. We study the spatial distribution and temporal behaviour of the Fe- $K\alpha$ emission with the objective of identifying the likely source of the excitation.

Methods. We have constructed an Fe- $K\alpha$ fluence map in a narrow energy band of width 128 eV centered on 6.4 keV. We use this to localize the brightest fluorescence features in the vicinity of the Arches cluster. We have investigated the variability of the 6.4-keV line emission of several clouds through spectral fitting of the EPIC MOS data with the use of a modelled background, which avoids many of the systematics inherent in local background subtraction. We also employ spectral stacking of both EPIC PN and MOS data to search for evidence of an Fe-K edge feature imprinted on the underlying X-ray continuum.

Results. The lightcurves of the Fe- $K\alpha$ line emission from three bright molecular knots close to the Arches cluster were found to be constant over the 8-year observation window. However, West of the cluster, we found a bright cloud which shows the fastest Fe- $K\alpha$ variability yet seen in a molecular cloud in the Galactic center region. The time averaged spectra of the molecular clouds revealed no convincing evidence of the 7.1-keV edge feature, albeit with only weak constraints. The *EW* of the 6.4-keV line emitted by the clouds near to the cluster was found to be ~ 1.0 keV.

Conclusions. The observed Fe- $K\alpha$ line flux and the high value of the *EW* suggest an origin of the fluorescence in the photoionization of the MCs by X-ray photons, although excitation by cosmic-ray particles is not specifically excluded. For the three clouds nearest to the Arches cluster, the identification of the source of these X-rays as an earlier outburst on Sgr A* is at best tentative, although not entirely ruled out by the observations. On the other hand, the hardness of the nonthermal component associated with the 6.4-keV line emission might be best explained in terms of the bombardment of the clouds by cosmic-ray particles emanating from the Arches cluster itself. The relatively short-timescale variability seen in the 6.4-keV line emission from the cloud to the west of the cluster is most likely the result of its X-ray illumination by a nearby transient X-ray source.

Key words. Galaxy: center – ISM: clouds – cosmic rays

1. Introduction

The Galactic center (GC) is a bright source of diffuse 6.4-keV fluorescent line emission corresponding to the $K\alpha$ transition in neutral iron (Fe) atoms (or low-ionization Fe ions). The spatial distribution of the line emission is clumpy, but at the same time widespread across the whole region, and shows a good correlation with that of molecular clouds (MCs) (Yusef-Zadeh et al. 2007a). The three regions which have the most prominent 6.4-keV line emission are Sgr B2 (Inui et al. 2009), Sgr C (Nakajima et al. 2009) and the molecular filaments between Sgr A* and the Radio Arc (Koyama et al. 2009). However, more than a decade after the discovery of this fluorescent emission (Koyama et al. 1996), the mechanism of its excitation remains a puzzle. The fluorescence may be the result of the irradiation of cold gaseous matter by hard X-rays photons with energies above 7.1 keV (the K-edge of neutral iron). Alternatively, the excitation might be through the bombardment of the gas by cosmic-ray (CR) particles with energies above this same threshold. In

both cases the removal of a K-shell electron, is rapidly followed by recombination and the emission of a fluorescent $K\alpha$ photon. In X-ray binaries and active galactic nuclei (AGNs), the observed 6.4-keV line is generally interpreted as the reprocessing of X-rays from the central X-ray continuum source at the surface of surrounding dense media, such as an accretion disc and/or a molecular torus (e.g., Fabian et al. 1989; Nandra et al. 1997). However, in the case of the fluorescing structures seen in the GC region, there is no obvious persistent source bright enough to explain the observed line fluxes. One possible solution to this paradox is that the X-ray illuminating source, from our offset perspective, is highly obscured. Alternatively, such a source may possibly have been bright in the past, but is currently faint.

The first observations of 6.4-keV emission from the GC (Koyama et al. 1996) prompted the suggestion that the required X-ray illumination might be associated with the past activity of Sgr A* (Sunyaev & Churazov 1998). In particular, Murakami et al. (2000) suggested, based on their X-ray study of the molecular cloud with the brightest 6.4-keV emission, Sgr B2, that

Table 1. Specifications for the selected OBSIDs.

OBSID	Obs Date yyyy-mm-dd	PN cut/GTI/exp	MOS1 cut/GTI/exp	MOS2 cut/GTI/exp
0111350101	2002-02-26	0.8/38.590/40.030	0.5/42.262/52.105	0.5/41.700/52.120
0202670501	2004-03-28	2.0/13.320/101.170	1.0/33.070/107.784	1.0/30.049/108.572
0202670601	2004-03-30	2.0/25.680/112.204	1.0/32.841/120.863	1.0/35.390/122.521
0202670701	2004-08-31	1.0/59.400/127.470	0.5/80.640/132.469	0.5/84.180/132.502
0202670801	2004-09-02	1.0/69.360/130.951	0.5/94.774/132.997	0.5/98.757/133.036
0402430301	2007-04-01	1.5/61.465/101.319	0.8/61.002/93.947	0.8/62.987/94.022
0402430401	2007-04-03	1.5/48.862/93.594	0.8/40.372/97.566	0.8/41.317/96.461
0402430701	2007-03-30	1.5/32.337/32.338	0.8/26.720/33.912	0.8/27.685/33.917
0505670101	2008-03-23	1.25/74.216/96.601	0.5/73.662/97.787	0.5/74.027/97.787
0554750401	2009-04-01	1.0/30.114/38.034	0.5/32.567/39.614	0.5/33.802/39.619
0554750501	2009-04-03	1.0/36.374/42.434	0.5/41.376/44.016	0.5/41.318/44.018
0554750601	2009-04-05	1.0/28.697/32.837	0.5/37.076/38.816	0.5/36.840/38.818

Notes. In each of the instrument related columns we report the threshold used for the good time interval (GTI) selection in the 10–12 keV lightcurve (in units of counts/s), the total GTI exposure and the nominal duration of each observation.

Sgr A* had been in an active phase roughly three hundred years earlier. This interpretation has remained in favour; for example, Terrier et al. (2010) have recently measured the decay of the lightcurve of the scattered X-ray continuum emanating from Sgr B2 and argue that this requires the period of intense activity of Sgr A* to have ended between 75 and 155 years ago. In this setting a key observational fact is that Sgr A* is currently some six orders of magnitude fainter than required (Baganoff et al. 2001). Even the brightest X-ray flares detected so far (amplitude 100–160, Porquet et al. 2003, 2008) are still 4 orders of magnitude fainter than required and have too short a duration (~ 1 h). The X-ray photon irradiation scenario is often referred to as the X-ray Reflection Nebulae (XRN) model, irrespective of whether Sgr A* is the actual source of the X-ray photon illumination.

An alternative to the XRN model is to invoke the incidence of CR electrons and/or protons as the excitation source (e.g. Predehl et al. 2003; Yusef-Zadeh et al. 2007a; Dogiel et al. 2009). Although low-energy ($E \lesssim 100$ keV) CR electrons are favoured over highly energetic particles (Yusef-Zadeh et al. 2002a), we note that the cross-section for the production of inner shell ionization of Fe atoms by ultra-relativistic (Lorentz factor $\gtrsim 100$) electrons is not negligible; in fact, it amounts to about 1% of the Fe-K photoionization cross-section (see Tatischeff 2003). In the case of protons, the cross-section for the ionization process is highest for subrelativistic particles (Dogiel et al. 2009).

One main way to distinguish between the two proposed scenarios is to investigate the temporal variability of the 6.4-keV line emitted from the GC MCs, since fast variability (typically on a timescale of a few years) in which reflection echos appear to propagate at roughly the speed of light, favours illumination by X-ray photons rather than by non-relativistic CR particles. Ponti et al. (2010) argued that the XRN model coupled with the hypothesised past activity of Sgr A*, provided a consistent explanation for the complex pattern of variability seen in the molecular filaments located between Sgr A* and the Radio Arc. However, it remains unclear whether or not CR particle bombardment also plays a role in the excitation of the X-ray fluorescence from at least some of these peculiar MCs. For example, the non-zero level of the Fe- K_{α} lightcurve prior to the onset of an episode of enhanced emission in the molecular complex known as the “Bridge” (Ponti et al. 2010), could be due to an underlying CR-induced line flux.

Here, we report an X-ray study of the MCs in the surroundings of the Arches cluster (AC) based on observations carried

out by *XMM-Newton*. This region was not studied in detailed in the recent *Chandra* and *XMM-Newton* compilations of 6.4-keV cloud properties (Muno et al. 2007; Ponti et al. 2010), although earlier *Chandra* results for the AC have been reported by Yusef-Zadeh et al. (2002b), Law & Yusef-Zadeh (2004), and Wang et al. (2006).

Throughout this paper, we assume the distance to the GC to be 8 kpc (Gillessen et al. 2009). In Sect. 2 of this paper we present the *XMM-Newton* observations and describe the data reduction techniques we have employed. In Sect. 3, we investigate the spatial distribution of the Fe- K_{α} line emission in the vicinity of the AC and select four bright regions for further temporal and spectral analysis. The study of the Fe- K_{α} line variability has been performed using background modelling, while for the spectral analysis of the time averaged spectra we employed a standard background subtraction technique. We then go on to discuss our results in the context of the two main scenarios proposed to explain the Fe fluorescent-line emission, namely the XRN model and the CR particle bombardment model (Sect. 4). Finally, Sect. 5 summarises our main results.

2. Observations and data reduction

We selected archival *XMM-Newton* data of the GC region largely targeted at Sgr A*. We reprocessed the data from both the PN and MOS cameras (Strüder et al. 2001; Turner et al. 2001) with the tasks EPPROC and EMPROC in the Science Analysis Software version 9.0. In order to mitigate the effects of occasional high particle background rates in the detectors, induced by bursts of soft protons incident on the satellite, we constructed the 10–12 keV lightcurve of the data from the whole field of view (FOV). A threshold was then set so as to cut all the peaks in the background rate, thereby defining the good time intervals (GTIs) for the time filtering of the observation. Since the selected observations were performed in varying conditions of internal/particle background and orbital phase, we investigated all the lightcurves independently and selected a threshold count rate separately for each observation/camera combination (see also Capelli et al. 2011). The specifics of the *XMM-Newton* observations employed in the present work are reported in Table 1. Throughout our analysis we have only selected single and double events (PATTERN ≤ 4) for the PN and up to quadruple events (PATTERN ≤ 12) for the MOS1 and MOS2 cameras. For all the instruments a further screening involved selecting only events marked as real X-rays (FLAG==0).

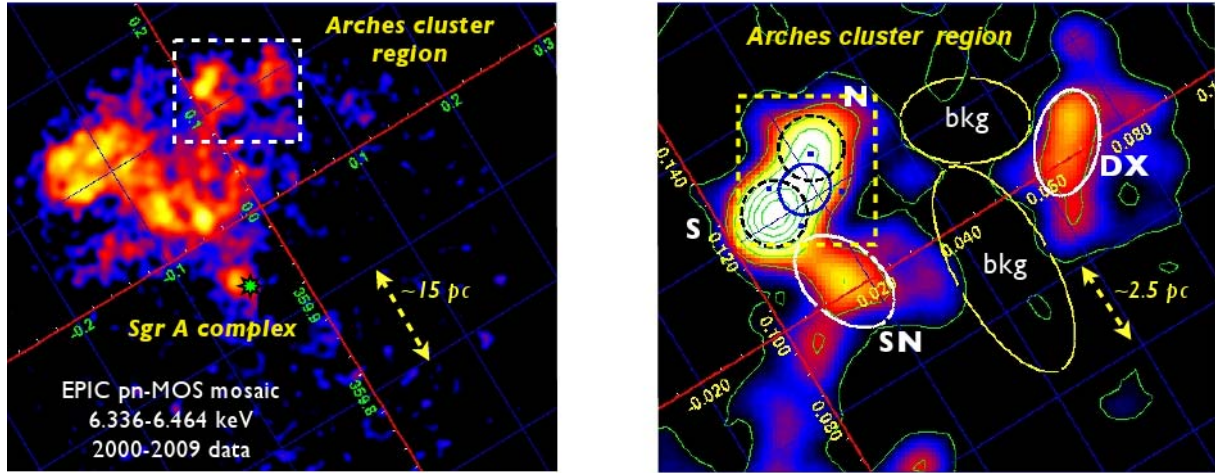


Fig. 1. *Left panel:* Fe- $K\alpha$ emission line map of the GC region. The data have been background subtracted and vignetting corrected. The position of Sgr A* is marked by a green star. The dashed white ellipse shows the AC region. *Right panel:* a zoom into the AC region. The position of the AC is indicated by the blue ellipse at $l \sim 0.12^\circ$, $b \sim 0.02^\circ$. Bright 6.4-keV knots are highlighted by dashed black circles (labelled N and S) and white ellipses (labelled SN at $b \sim 0.015^\circ$ and DX at $b \sim 0.07^\circ$). The region used for background accumulation is shown by the two yellow ellipses (bkg). The dashed yellow box shows the sky region studied in Wang et al. (2006, Fig. 14). The galactic coordinate grid is shown in red.

3. Analysis and results

3.1. The spatial distribution of the 6.4-keV line and its association with MCs

A first task was to construct a fluence (integrated flux over time) map for the Fe- $K\alpha$ line in a narrow spectral window from which we might hope to identify and locate the brightest fluorescence regions. We merged the GTI-filtered event files for the three EPIC cameras (where available) for each observation, using the SAS task EMOSAIC. In building the image of the Fe- $K\alpha$ emission, we assumed a value of $E/\Delta E = 50$ at 6.4 keV for the spectral resolution ($FWHM$) of both the PN and MOS1/2 cameras, corresponding to a bandpass for the Fe fluorescence signal of 6336–6464 eV. The resulting map of the 6.4-keV line emission is shown in the left panel of Fig. 1; the AC is located at the edge of the *XMM-Newton* FOV at the position RA = $17^{\text{h}}45^{\text{m}}40.045^{\text{s}}$, Dec = $-29^{\circ}0'27.9''$. The general distribution of the Fe fluorescent emission evident in this figure is very similar to that previously reported from both *XMM-Newton* (Predehl et al. 2003) and Suzaku (Koyama et al. 2009) observations.

Yusef-Zadeh et al. (2003) studied the non-thermal emission in the locality of the AC and showed that the giant non-thermal filament of the Radio Arc ($l \sim 0.2^\circ$) runs to the East of the AC with smaller thermal filaments lying to the North. The non-thermal emission originates in synchrotron radiation emitted by relativistic electrons in the strong magnetic fields within the Radio Arc structure. Examination of a broadband (2–10 keV) version of Fig. 1 shows that the general profile and extent of the AC inferred from the *XMM-Newton* data is in good agreement with previous *Chandra* measurements (Yusef-Zadeh et al. 2002b; Law & Yusef-Zadeh 2004; Wang et al. 2006). The AC morphology consists of a northern core component (designated as A1 and A2 in Yusef-Zadeh et al. 2002b) and a southern extended component (A3 in Yusef-Zadeh et al. 2002b). *XMM-Newton* separates these north and south continuum components but is unable to resolve structures within them. The right panel of Fig. 1 shows that there are three regions relatively close to the AC which can be identified as distinct sources of 6.4-keV fluorescence. Two of these regions coincide with the north (N) and south (S) continuum components defined above. The third is located to the south-west of the S component (labelled as region

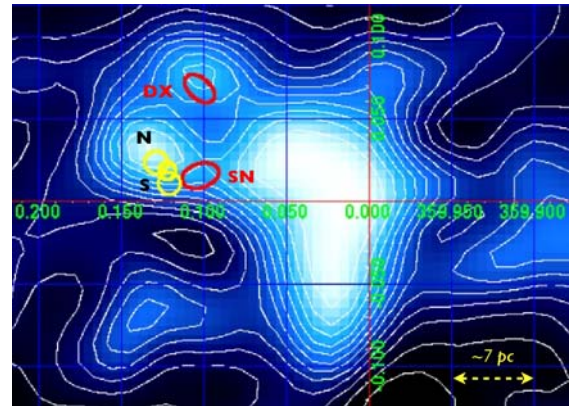


Fig. 2. Intensity map in galactic coordinates of the CS $J = 1-0$ line (Tsuboi et al. 1999) integrated over the velocity range -40 km s^{-1} – 0 km s^{-1} . The locations of the four bright knots identified in the *XMM-Newton* Fe- $K\alpha$ image are also indicated.

SN). Moreover, the *XMM-Newton* observations also reveal a 6.4-keV bright knot further to the west of the N component (labeled as region DX).

There are some notable differences between the Fe- $K\alpha$ line emission map obtained with *XMM-Newton* (Fig. 1, right panel) and the one measured by *Chandra* (Wang et al. 2006). First, *XMM-Newton* detected a northern 6.4-keV feature (knot N) close to the AC itself, which was not seen in the equivalent *Chandra* line image. With the higher statistics and the larger effective area of EPIC cameras, we also discovered a prominent tapered feature (knot SN) that seems to be connected to the knot S region.

To identify possible molecular counterparts to the Fe- $K\alpha$ bright knots we used data from the CS $J = 1-0$ (48.99 GHz) survey of the Central Molecular Zone (CMZ) (Tsuboi et al. 1999). The results are shown in Fig. 2, where the blue colour scale and the contours represent the CS $J = 1-0$ line emission intensity integrated over the -40 km s^{-1} to 0 km s^{-1} velocity range. The locations of the bright 6.4-keV knots are also indicated. A CS enhancement at $l \sim 0.13^\circ$, $b \sim 0.03^\circ$ coincides positionally with knot N. This molecular feature has a velocity of -30 km s^{-1} . Lower surface brightness molecular structures are

Table 2. Physical properties of the 6.4-keV emitting clouds.

Cloud	Size (pc)	$N_{\text{H}}(\text{cm}^{-2})$	#H (10^{59})	τ_{T}
N	0.92	4×10^{22}	9.6	0.0266
S	0.92	2×10^{22}	4.8	0.0133
SN	1.6×1.0	2×10^{22}	9.0	0.0133
DX	1.5×0.9	2×10^{22}	7.6	0.0133

Notes. Here, we report the cloud size in parsecs (in radius or semi-axis), the equivalent H column density through the cloud, the estimated total number of H atoms inside the cloud and the optical depth of the cloud to Thomson scattering.

also seen close to the SN and DX knots. We note that the CS emission at the four knot locations spans a spread of velocities which, although narrow enough to likely rule out the possibility that the molecular material is widely distributed along the line of sight, is sufficiently broad to suggest that the dynamics of the MCs in this region are dominated by turbulence.

Hereafter, we take the view that the four 6.4-keV knots represent coherent molecular structures in the vicinity of the AC. On this basis, Table 2 details the physical parameters of each MC. The angular size of the clouds have been estimated by eye and then converted to a linear size. For the hydrogen column density through the N and S clouds, N_{H} , we use the values reported by Amo-Baladrón et al. (2009) which in turn were derived from CS molecular emission. Because these authors did not report the equivalent H column densities for the other two knots, we assumed these to be the same as the region S (since the emission contours of the CS $J = 1-0$ line, at the locations of these knots are similar to those in the S region). We caution that the estimate of the N_{H} of a MC in the GC is strongly dependent on the method used to measure it. For example, for the large G0.13-0.13 molecular complex, two extreme values have been inferred for N_{H} , namely $4 \times 10^{22} \text{ cm}^{-2}$ (Amo-Baladrón et al. 2009, using CS $J = 1-0$ line) and a much higher value of 10^{24} cm^{-2} (Handa et al. 2006, based on the H^{13}CO^+ $J = 1-0$ line). Finally, we calculated the number of H atoms in the MCs and the value of the optical depth for Thomson scattering (τ_{T}). The estimates in Table 2 will be used in Sect. 4 to investigate the origin of the Fe- K_{α} line emission.

3.2. Fe- K_{α} line flux and variability – background modeling

We are interested in determining both the absolute photon flux in the Fe- K_{α} line and in searching for temporal variability in this signal. To this end, we extracted the spectra for each of the four bright 6.4-keV knots for each observation and then, for observations separated by only a few days, combined the data to give a sampling at six epochs as follows: February 2002 (1 observation), March 2004 (2 observations), August/September 2004 (2 observations), March/April 2007 (3 observations), March 2008 (1 observation), and April 2009 (3 observations).

The 6.4-keV emitting knots are not visible in the full band (2–10 keV) X-ray image, since their continuum signal is hard to distinguish against the strong diffuse X-ray emission which permeates the GC region. Indeed, the main contribution to the 2–10 keV spectrum of these extended sources is the thermal emission from the GC region. The best choice in performing a self-consistent spectral analysis of these low surface brightness features is to model the background as a component within the spectral fitting rather than subtracting it prior to the fitting. This technique avoids many systematic errors due to the

contamination by foreground emission (De Luca & Molendi 2004; Leccardi & Molendi 2008), but has the disadvantage that we are forced to exclude PN data (since at present, no detailed study of the instrumental background for the PN EPIC-camera has been provided).

The model used in the spectral fitting accounts for:

- Photoelectric absorption (WABS, Morrison & McCammon 1983). All the emission components are subject to soft X-ray absorption so as to account for the high column density along the line of sight to the GC region.
- Galactic thermal diffuse emission ($2 \times \text{APEC}$, Smith et al. 2001). Two thermal components are needed to explain the spectral shape of the GC thermal emission: one *warm* with a temperature of ≈ 1 keV (Ryu et al. 2009) and one *hot* with a temperature in the range 5–7 keV (Koyama et al. 2007). The higher temperature plasma is needed to constrain the fit in the region of Fe-line complex. The metallicities of the two thermal plasmas have been fixed to twice solar. Tanaka (2002) showed that the equivalent width of the S and Fe lines in the spectrum of the Galactic Ridge decrease as one moves away from the GC, with higher than solar metallicities required for elements such as Si, S and Fe in the diffuse plasma permeating the GC region. Recently, Nobukawa et al. (2010) also measured a supersolar metallicity for the hot plasma in the GC region. The twice solar constraint results in a broadly satisfactory fit to all our spectra, whereas use of a solar metallicity produces high residuals in all the soft X-ray (i.e., $\lesssim 3-4$ keV) emission lines.
- The Cosmic X-ray Background (POWER-LAW). The spectral shape of this component is modelled as a power-law continuum with a photon index fixed at $\Gamma = 1.4$ (Hickox & Markevitch 2007). The normalization of this component was set to $10.9 \text{ photon cm}^{-2} \text{ s}^{-1} \text{ sterad}^{-1} \text{ keV}^{-1}$ (Hickox & Markevitch 2007).
- A non-thermal hard X-ray component (POWER-LAW). The non-thermal continuum emission directly linked to the Fe-line fluorescence. We fixed the slope of the power-law component associated with the source of fluorescence to $\Gamma = 1$ in order to give consistency in the measurement of the 6.4-keV flux across the different datasets¹.
- Fe fluorescent lines (2 GAUSS). The two spectral lines with gaussian profiles were used to represent the Fe- K_{α} and Fe- K_{β} fluorescent lines at 6.4 keV and 7.05 keV. The flux of the Fe- K_{β} line was fixed at 0.11 times that of the K_{α} component (Koyama et al. 2009).
- The particle background (POWER-LAW). We used the values reported in Leccardi & Molendi (2008) for the slopes of the particle component in the MOS1 and MOS2 spectra, respectively $\Gamma = 0.24$ and $\Gamma = 0.23$. Since this instrumental background is not focused in the detector, it does not need to be convolved with the instrument response.

The statistics of each spectrum (per region, per epoch) differ markedly from one another. Since the construction of the lightcurves of the 6.4-keV line flux must be done in a consistent way, we decided to fix the temperature of the hot plasma component at 6.5 keV (Koyama et al. 2007), given that variations

¹ The value of Γ was chosen after studying the stacked spectrum of region S (see Sect. 3.3), which shows the most intense 6.4-keV line emission, and therefore has the best statistics. This analysis gave $\Gamma = 1.0^{+0.1}_{-0.2}$ consistent with earlier estimates from *Chandra* ($\Gamma = 1.3^{+1.4}_{-1.1}$) and *Suzaku* ($\Gamma = 0.72^{+0.68}_{-0.72}$) (respectively, Wang et al. 2006; Tsujimoto et al. 2007).

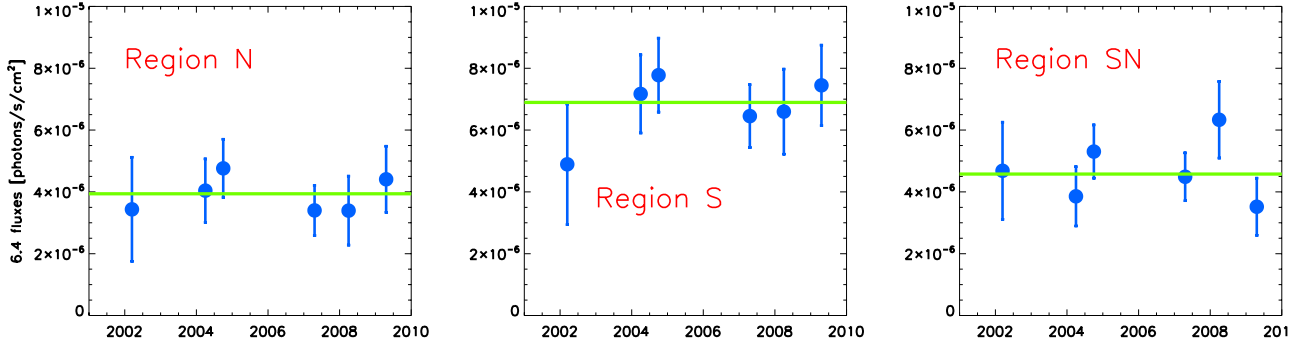


Fig. 3. Lightcurves of the Fe- $K\alpha$ line flux from the MCs in the vicinity of the AC. The flux values are in units of 10^{-6} photons/cm²/s. The green horizontal lines show the weighted means of the data points.

Table 3. Fluxes of the Fe- $K\alpha$ line.

Region	Feb02	Mar04	Sep04	Apr07	Mar08	Apr09	Wtd Mean	χ^2_{red}
N	3.4 ± 1.7	4.0 ± 1.0	4.8 ± 1.0	3.4 ± 1.0	3.4 ± 1.1	4.4 ± 1.1	3.9 ± 0.4	0.4
S	4.9 ± 1.9	7.2 ± 1.3	7.8 ± 1.2	6.5 ± 1.0	6.6 ± 1.4	7.4 ± 1.3	6.9 ± 0.5	0.4
SN	4.7 ± 1.6	3.9 ± 1.0	5.3 ± 0.9	4.5 ± 0.8	6.3 ± 1.2	3.5 ± 0.9	4.6 ± 0.4	0.9
DX	1.2 ± 1.1	3.1 ± 0.9	4.7 ± 0.9	3.3 ± 0.7	1.9 ± 0.8	1.7 ± 0.7	2.7 ± 0.3	2.1

Notes. The values reported in the table are the weighted means of the MOS1&2 measured fluxes, in units of 10^{-6} photons/cm²/s. The different columns refer to different datasets (see text). The Apr07, Mar08 and Apr09 fluxes for region D are based on MOS 2 data only, as a consequence of the damaged sustained by CCD6 in MOS 1 on 9 March 2005 (Abbey et al. 2006).

in the temperature of this component have the potential to unduly influence the measured Fe $K\alpha$ line flux. Note, however, that the temperature of the warm thermal emission was taken to be a free parameter, as were the normalizations of the two thermal plasma components. The warm component temperature ranges inferred for the N, S and SN clouds are 0.5–2 keV, 0.7–1.3 keV and ~ 1 keV respectively, values which are in good agreement with those obtained in Sect. 3.3 from the analysis of the stacked spectra. These temperatures are marginally lower than the value of 1.7 keV measured for the core of the AC (Capelli et al. 2011), hinting at a decrease in the warm plasma temperature as one moves away from the cluster until an “ambient” medium with $kT \approx 1$ keV is reached. Because of the reduced signal to noise ratio, all the spectra of the DX region were fitted with the warm plasma temperature fixed at the ambient value, (i.e. $kT = 1$ keV).

Because of the different slopes of the particle component in the MOS cameras, the MOS1 and MOS2 spectra were kept separate, giving two spectral datasets for each of the four regions (N, S, SN, DX) for each of the six epochs. Given the restricted photon statistics, we used the Cash statistic rather than the χ^2 . Prior to spectral fitting we grouped the channels in each spectrum with the GRPPHA tool in order to have a minimum of 1 count/bin (De Luca & Molendi 2004). The photon fluxes in the 6.4-keV line determined from this analysis are reported in Table 3. In the last two columns of this table we also report the weighted mean across the six measurement epochs and the reduced χ^2 for the constant flux hypothesis. Figure 3 shows the lightcurves of the 6.4-keV line for the three MCs in the immediate vicinity of the AC, together with the weighted mean flux. We find that the 6.4-keV line fluxes from all of these knots (regions N, S and SN) are constant with time.

The DX cloud is ~ 3 arcmin (about 7 pc in projection) to the West of the AC, in a region which appears to be disconnected from the cluster itself and from the other 6.4-keV bright knots studied in this paper. The lightcurve of the Fe $K\alpha$ emission from

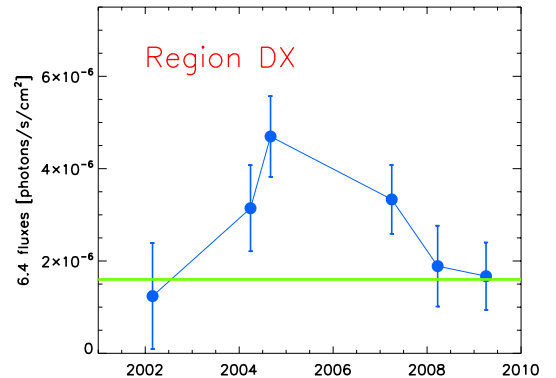


Fig. 4. Lightcurve of the 6.4-keV line for the DX cloud. The weighted mean ($1.6 \pm 0.5 \times 10^{-6}$ photons/cm²/s) of the first and last data points is shown as the horizontal green line. The emission reaches a maximum in September 2004 with a line flux roughly three times the base level.

the DX cloud shows clear evidence for time variability (Fig. 4), which is supported by the high value of χ^2_{red} for these data with respect to the constant flux hypothesis (Table 3). Clearly, the temporal behavior of this particular cloud is very different to that of the three bright knots closer (in projection) to the AC. Its temporal behaviour is also different to that reported for all the other MCs in the GC (Inui et al. 2009; Ponti et al. 2010). In the DX knot we clearly see both an increase and decrease in the Fe fluorescent flux rather than solely an increasing (or decreasing) trend over the monitoring period. The Fe- $K\alpha$ flux from this cloud appears to have increased by a factor of three over a period of about 2.5 years with a peak in September 2004 after which, over a timescale of a few years, it faded back to its pre-outburst level. Interestingly the average of the first and last points in the lightcurve is not zero, suggesting that the outburst was superimposed on a base level. The variability exhibited by this cloud is the *fastest* yet reported for the GC region.

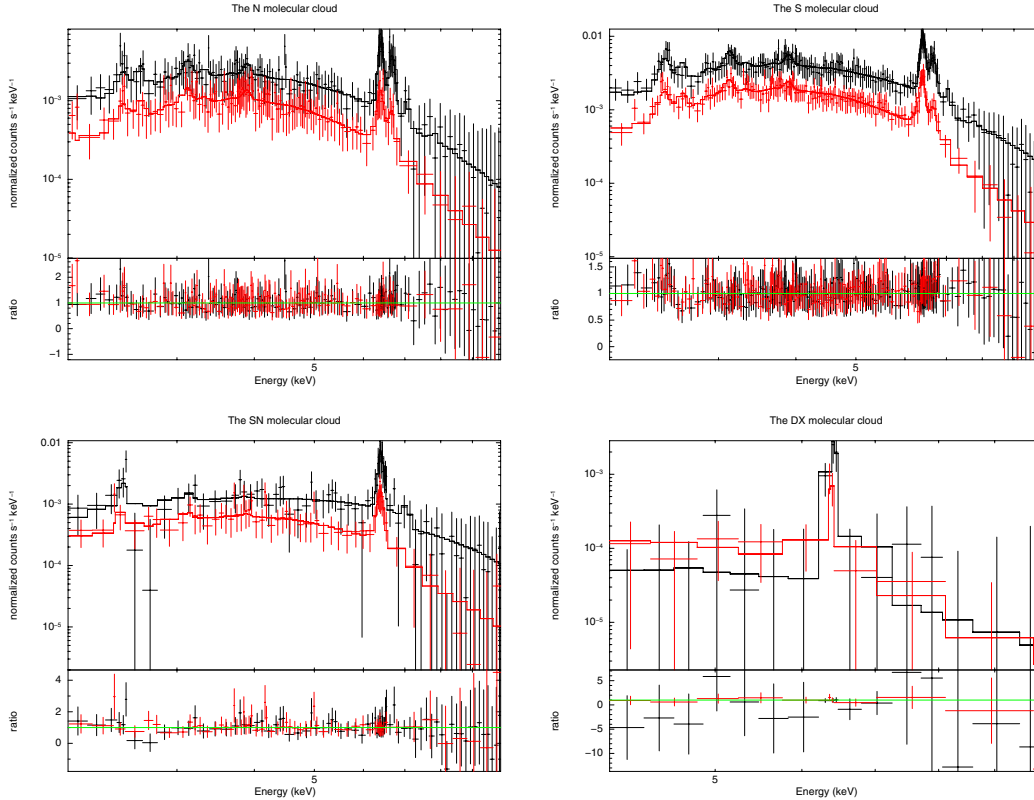


Fig. 5. PN (black) and MOS (red) stacked spectra of the four selected MCs in the 2–10 keV (4–10 keV for the DX cloud) energy range, together with the ratio between the data points and the best fit model. The *top panels* show the spectra of the N and S molecular complexes, with the *bottom panels* similarly presenting the spectra of SN and DX clouds.

3.3. Analysis of the time averaged spectra – stacking + background subtraction

We have also carried out an analysis of the stacked PN and MOS spectra of the four 6.4-keV knots with the objective of determining the equivalent width (EW) of the Fe- K_{α} fluorescent line with respect to the associated continuum. A second objective was to check for an Fe-K absorption edge at 7.1 keV imprinted on the same continuum (Sunyaev & Churazov 1998; Murakami et al. 2000). Because of the stacking of the data (i.e. the addition of all the spectra across the set of observations), the photon statistics were much improved, which allowed us to employ a more standard background subtraction technique and therefore include the EPIC-PN data in the study. We again used the C-statistics because of the low number of counts per bin in the spectra; indeed, when fitting with the χ^2 statistics the χ^2_{red} values are always too small (about 0.2–0.3) to be confident with the best fit results. Moreover, for what concerns the spectral analysis of the MCs in the vicinity of the AC, we notice that the C-statistics give always tighter constraints on the spectral parameters.

The background spectra for the PN and MOS channels were built by stacking all the background spectra collected for the different datasets. The region selected for the background accumulation corresponds to the two ellipses with semi-axes 0.8×0.5 arcmin and 1.4×0.6 arcmin shown in the right panel of Fig. 1. The spectral model used to fit the data comprises a collisional ionized *warm* plasma (APEC, with temperature and normalization free parameters) and a power-law continuum with associated Fe- K_{α} and Fe- K_{β} lines at 6.4 and 7.05 keV ($K_{\beta}/K_{\alpha} = 0.11$). All the emission components were then subject to absorption in the ISM along the line of sight (WABS, common to both the APEC and the power law). For this analysis the slope of the

non-thermal continuum radiation associated with the fluorescence was again fixed at $\Gamma = 1$. The use of a local background removes the requirement for two of the spectral components included previously, namely the hot thermal component and the cosmic X-ray background, both of which can be assumed to have constant surface brightness across the AC region.

The results are summarised in Fig. 5 and Table 4². Regions N and S have rather similar spectra, in which contamination by residual thermal emission (not removed by the background subtraction) is clearly present in the form of the helium-like Fe line at 6.7 keV and other helium-like lines of other elements (S, Ar, Ca) at lower energies. In these regions, close to the AC core, we derive a temperature of the *warm* plasma consistent with that previously measured in the core (Wang et al. 2006; Tsujimoto et al. 2007; Capelli et al. 2011). The X-ray spectra of both complexes exhibit high line-of-sight absorption and a relatively high EW for the neutral iron Fe K_{α} line (~ 1.0 keV). The high value of the EW might be interpreted as evidence for X-ray irradiation as the origin of this fluorescence. For this reason, we also investigated whether there is any evidence for the

² The values quoted here are based on the MOS data only. We do not consider the PN values here because of likely systematic errors in the background subtraction. The fluxes of the 6.4-keV line in the background-subtracted PN spectra are generally lower than those determined from the equivalent MOS spectra such that, if the PN measurements are included, then the line fluxes based on the stacked spectra are not consistent with the MOS-only values derived in Sect. 3.2. We tried also to fit the stacked PN spectra modeling the background with a simple powerlaw component ($\Gamma = 0$), and got consistent results, both between PN and MOS cameras, and with the fluxes measured in Sect. 3.2. Therefore, we associate these systematics in PN measurements of the 6.4-keV emission to the background subtraction.

Table 4. Results for the spectral analysis of the stacked spectra.

	N	S	SN	DX
N_{H}	9.5 ± 1.5	10.1 ± 0.7	$8.5^{+4.0}_{-3.4}$	6.0 (fixed)
kT (keV)	1.8 ± 0.3	1.6 ± 0.1	$1.0^{+1.0}_{-0.5}$	–
norm_{kT}	$4.7^{+2.4}_{-1.5}$	$9.2^{+2.5}_{-2.4}$	$2.8^{+17.7}_{-2.4}$	–
$F_{6.4}$	3.2 ± 0.5	6.2 ± 0.6	3.2 ± 1.0	1.9 ± 0.5
norm_{POW}	2.0 ± 0.3	4.4 ± 0.4	$1.8^{+0.4}_{-0.2}$	0.5 ± 0.1
τ	≤ 0.4	≤ 0.6	≤ 1.8	–
$EW_{6.4}$	1.0 ± 0.4	0.9 ± 0.2	1.1 ± 0.4	$2.6^{+2.1}_{-1.1}$
C-stat	2337.60	2280.52	2335.05	453.92

Notes. Here we report the total column density (N_{H} , in 10^{22} cm^{-2}) inferred from the X-ray measurements, the temperature and the normalization of the APEC thermal plasma (in units of $10^{-18} \int n_e n_{\text{H}} dV / 4\pi D^2$, where n_e and n_{H} are the electron and H densities in cm^{-3} , and D the distance to the source in cm), the flux of the Fe $K\alpha$ line (in units of $10^{-6} \text{ photons/cm}^{-2}/\text{s}$), the normalization of the powerlaw component ($10^{-5} \text{ photons/keV/cm}^{-2}/\text{s}$ at 1 keV), the EW of the Fe- $K\alpha$ line (in keV) with respect to the powerlaw component, the upper limit to the optical depth of the Fe-K edge, and the C-stat values for the best fit model (the degrees of freedom are 2119 for the regions N, S and SN, 397 for the region DX).

Fe-K absorption edge, by applying a multiplicative EDGE model (with a fixed energy of 7.1 keV) to the power-law continuum component; however, on the basis of the spectral fitting there was no requirement for such a feature. We could only measure an upper limit to the optical depth of this absorption edge (see Table 4). However, the detection of an optical depth of about 0.1–0.2 (equivalent to $N_{\text{H}} \sim 10^{23} \text{ cm}^{-2}$) at the Fe-K absorption edge energy (7.1 keV) is challenging when the statistics are limited and the spectrum above 7 keV is potentially contaminated by systematic errors in the subtraction of the instrumental background (which has a non-uniform pattern in the detector).

The spectral parameters inferred for the SN region are similar to those obtained for the N and S clouds, except for the marginally lower temperature inferred for the warm plasma ($kT \sim 1 \text{ keV}$) which, as noted earlier, may plausibly be a consequence of the increased distance from the AC core. A high value for the EW of the 6.4 keV line ($EW \sim 1.1 \text{ keV}$) is again evident, with no requirement for an absorption edge at 7.1 keV.

In the case of the DX cloud the derived spectrum, which is shown in the lower right panel of Fig. 5, is very strongly photon limited. In fact the statistics are so poor that no net signal was detected below 4 keV and no warm plasma component was required in the fit. The inferred 2–10 keV photon flux based on the spectral fitting was $5.9 \pm 3.5 \times 10^{-6} \text{ photons/cm}^2/\text{s}$, that is almost an order of magnitude lower than the continuum fluxes inferred for the other knots. The measurement of an Fe-K absorption edge could not be done.

3.4. Summary of the results

The results of Sect. 3 can be summarized in five main points:

- Fe- $K\alpha$ line variability (N-S-SN): the lightcurve of the 6.4-keV line flux has been found to be constant in the regions N, S and SN;
- Fe- $K\alpha$ line variability (DX): we measured a fast variability of the Fe fluorescent line in the DX cloud, with a timescale of about 2–3 years;

- EW of the 6.4-keV line: all four MCs studied have high values ($\sim 1 \text{ keV}$) for EW of the Fe fluorescent line, although the errors, particularly for the DX cloud, are relatively large. Unfortunately, the 90% confidence range for the EW is too wide to place tight constraints on the excitation mechanism of Fe fluorescence;
- Fe-K edge at 7.1 keV: we failed to detect an absorption edge imprinted on the power-law component in any of the MCs - much better statistics would be required to properly constrain the optical depth of such a feature;
- hardness of the non-thermal emission: we measured a hard spectral slope for the non-thermal emission for the region S (i.e. $\Gamma = 1.0^{+0.1}_{-0.2}$) with the spectra of the other clouds compatible with the presence of such a component.

4. Discussion

The CMZ contains approximately 10% of the molecular gas of the entire Galaxy largely in the form of dense clouds (Morris & Serabyn 1996). The bright Fe- $K\alpha$ line emission at 6.4 keV is a peculiar feature of the MCs located within this region. The 6.4-keV line is produced by the fluorescence of neutral (or near-neutral) Fe atoms subject to irradiation by hard X-rays (with energies above the Fe-K edge at 7.1 keV) and/or bombardment by CR particles with energies in the range from 7.1 keV up to, potentially, many 100's of keV. More than a decade after its first detection, the combination of circumstances which give rise to the bright Fe- $K\alpha$ emission in the GC remains a matter of discussion (e.g. Yusef-Zadeh et al. 2007a; Koyama et al. 2009; Dogiel et al. 2009). In a recent development, Munro et al. (2007) and Ponti et al. (2010) have studied the variability of the 6.4-keV line flux seen in several MCs lying between Sgr A* and the GC Radio Arc. These authors interpret their results in terms of the photoionization of molecular material by hard X-rays produced in a past (~ 100 years ago) bright ($L_{2-10} \sim 10^{39} \text{ erg/s}$) flare on the SMBH at the center of the Galaxy. On the other hand, some authors are not fully convinced by the Sgr A* outburst model (e.g., Predehl et al. 2003; Yusef-Zadeh et al. 2007a; Dogiel et al. 2009).

Here, we interpret the results of our study of four 6.4-keV bright knots located within ~ 3 arcmin of the AC. Projected onto the plane of the sky the separation of these knots from the AC is no more than ~ 7 pc; however, we have limited information on the relative line-of-sight locations, so the association of these structures with the AC is only tentative.

4.1. The XRN hypothesis

The three knots closest (in projection) to the AC exhibit a constant Fe- $K\alpha$ line flux and it is tempting to imagine that the AC itself might be the source of the excitation, whether via photons or particles. However, in the case of the former the average X-ray luminosity of the AC is nowhere near sufficient to produce the total amount of fluorescence observed. On the other hand, if the AC entered a putative high activity state in which its X-ray luminosity exceeded 10^{37} erg/s , then it would be possible to explain the observed 6.4-keV fluxes of the nearby clouds in the context of the XRN model. Capelli et al. (2011) recently reported X-ray flaring activity within the AC, most likely originating from stellar winds interactions in one or more massive binary systems, but even at its peak the measured luminosity remains three order of magnitude lower than that cited above. An alternative is to consider the temporary brightening of an X-ray

Table 5. Cloud parameters and distances inferred in the XRN/Sgr A* outburst model.

Cloud	N				S				SN				DX			
z	$1 z_{\odot}$	$1.25 z_{\odot}$	$1.5 z_{\odot}$	$2 z_{\odot}$	$1 z_{\odot}$	$1.25 z_{\odot}$	$1.5 z_{\odot}$	$2 z_{\odot}$	$1 z_{\odot}$	$1.25 z_{\odot}$	$1.5 z_{\odot}$	$2 z_{\odot}$	$1 z_{\odot}$	$1.25 z_{\odot}$	$1.5 z_{\odot}$	$2 z_{\odot}$
R	0.92	0.92	0.92	0.92	0.92	0.92	0.92	0.92	1.27	1.27	1.27	1.27	0.90	0.90	0.90	0.90
$F_{6.4}$	3.9	3.9	3.9	3.9	6.9	6.9	6.9	6.9	4.6	4.6	4.6	4.6	4.7	4.7	4.7	4.7
Ω	7.6	6.1	5.1	3.8	26.8	21.4	17.9	13.4	17.9	14.3	11.9	8.9	18.0	14.4	12.0	9.0
d	52.8	58.9	64.4	74.6	28.1	31.4	34.4	39.7	47.5	53.1	58.2	67.3	33.5	37.5	41.1	47.4
d_p	27.6	27.6	27.6	27.6	26.3	26.3	26.3	26.3	23.3	23.3	23.3	23.3	27.5	27.5	27.5	27.5
$d_{l.o.s.}$	45.0	52.0	58.2	69.3	9.9	17.2	22.2	29.7	41.4	47.7	53.3	63.1	19.2	25.5	30.5	38.6

Notes. Here, Z is the metallicity assumed for the MC, R the radius of the cloud as seen from Sgr A* (pc), $F_{6.4}$ the flux measured in the Fe-K $_{\alpha}$ line (photons/cm²/s), Ω the solid angle (scaled to the whole sky, in units of 10⁻⁵) subtended by the MC from the perspective of Sgr A*, d (pc) the distance of the MC from Sgr A*, d_p (pc) and $d_{l.o.s.}$ (pc) the distance projected onto the plane of the sky and along the line of sight, respectively.

binary source close to or even within the AC. Then the requirement is for the bright state to have lasted for more than 8 years at or above $L_x \sim 10^{37}$ erg/s; this is much longer than the typical flaring timescales of X-ray transient sources (e.g., [Degenaar & Wijnands 2010](#)).

4.1.1. Fe-K $_{\alpha}$ variability

In the XRN scenario, it has been conjectured that the most plausible source of hard X-ray photons is Sgr A*. On the basis of this assumption, we have investigated the possible distribution along the line of sight of the 6.4-keV clouds in the AC vicinity. In the following calculations, we assumed the X-ray luminosity of the Sgr A* giant flare to have been 1.4×10^{39} erg/s ([Ponti et al. 2010](#)). We then infer the physical separation between the clouds and Sgr A* using the formula reported in [Sunyaev & Churazov \(1998\)](#) which, to better fit our purposes, can be written in the form

$$\frac{R^2}{4d^2} = \Omega = \frac{4\pi D^2 \cdot F_{6.4}}{\tau \cdot L_x \times 10^7 \cdot Z} = 5.17 \times 10^{-4} \left(\frac{F_{6.4}}{10^{-4}} \right) \left(\frac{0.1}{\tau} \right) \left(\frac{Z_{\odot}}{Z} \right).$$

In this equation D is the distance to the GC (assumed to be 8 kpc), $F_{6.4}$ is the Fe-K $_{\alpha}$ line flux (in photons/cm²/s), τ the optical depth to Thomson scattering of the cloud, and L_x the X-ray luminosity of the Sgr A* flare. The solid angle Ω is defined as $\Omega = R^2/4d^2$, where R is the radius of the cloud as seen from Sgr A* (basically, the minor axis for the cloud DX and a combination of major and minor axis for the region SN, as measured on the sky) and d is the distance of the cloud from Sgr A* (Ω is scaled to be the fraction of the whole sky subtended by the MC from the perspective of Sgr A*).

By first determining Ω , we are then able to estimate d from the cloud dimension (assuming spherical symmetry). By comparison of d with the projected distance of the cloud from Sgr A* on the plane of the sky (d_p), we can then derive the position of the clouds along the line of sight relative to Sgr A* ($d_{l.o.s.}$).

Our calculations are, of course, highly dependent on the assumed past luminosity of Sgr A*. However, since we use the best estimate available based on the XRN modelling of other GC clouds ([Ponti et al. 2010](#)), we are in effect testing this model for internal self-consistency. However, the inferred line of sight location of the clouds ($d_{l.o.s.}$) will depend on the assumed metallicity (Z) of the molecular material (more specifically on the iron abundance) and also on the optical depths of the MCs. In the literature, there is not yet a consensus on the typical values of these parameters for MCs in the CMZ. In the case of the metal abundance, the best estimate is for supersolar values, closer to $Z = 2$ than $Z = 1$ ([Morris & Serabyn 1996](#)).

All the assumptions and the results of our calculations are detailed in Table 5. The Fe-K $_{\alpha}$ line fluxes for the different clouds are assumed as in the weighted mean column of Table 3; because of the measured variability, only for the DX cloud we assumed the peak flux measured in September 2004 (see Table 3) of 4.7×10^{-6} photons/cm²/s. The inferred geometry of the clouds distribution is shown in Fig. 6. Here, the cloud locations relative to Sgr A* are shown projected onto the Galactic plane with the y -axis representing the direction along the line of sight. The two parabolas correspond to curves of constant light path, representative of the leading and trailing edges of the inferred outburst on Sgr A*, as discussed by [Ponti et al. \(2010\)](#). The panels in Fig. 6 illustrate the impact of different assumptions with respect to the metallicity of the MCs.

We first consider the three clouds close to the AC (in projection), namely the N, S and SN clouds. Assuming a solar metallicity for the MCs, we infer line of sight displacements relative to Sgr A* ($d_{l.o.s.}$) of 45, 9.9 and 41.4 pc for the N, S and SN knots (Fig. 6, upper left panel). In this scenario we have the N and SN clouds placed in the region between the two parabolas and therefore currently illuminated by the Sgr A* outburst. A relatively constant 6.4-keV line flux is consistent with this model (assuming that Sgr A* remained in a relatively constant high state for the duration of the outburst). On the other hand, the cloud S is being crossed by the trailing edge of the irradiation burst. Therefore, one might expect that its Fe-K $_{\alpha}$ line flux to exhibit similar behaviour to that seen in the Sgr B2 and G0.11-0.11 MCs ([Inui et al. 2009](#); [Ponti et al. 2010](#), respectively), i.e., a steady decrease with time. Since such a decrease is not observed, there is clearly some inconsistency in the model based on the solar metallicity assumption. Moreover, we notice that the molecular complexes N and S are probably dense regions within the same larger MC (the -30 km s⁻¹ MC, see Fig. 14 in [Wang et al. 2006](#)); therefore, the relative separation of these two complexes by about 30–40 pc along the line of sight seems unlikely.

We therefore repeated the calculations assuming different Fe abundances; the values we considered are 1.25, 1.5 and 2 times solar ($d \propto Z^{0.5}$). The results of these calculations are detailed in Table 5, and illustrated in Fig. 6. We find that for a metallicity higher than 1.5, the XRN model again has problems in explaining the constancy of the Fe-K $_{\alpha}$ lightcurves of all the clouds. In the case of $Z = 1.5$, while the clouds S and SN lay well within the outburst region, the N cloud is at its leading edge (lower left panel), implying an increasing fluorescence signal (a behavior similar to the one measured from the *bridge* in [Ponti et al. 2010](#)). When $Z = 2$ (lower right panel) although the S region lies within the outburst region, the incident ionizing front propagating from Sgr A* has not yet reached the N and SN knots.

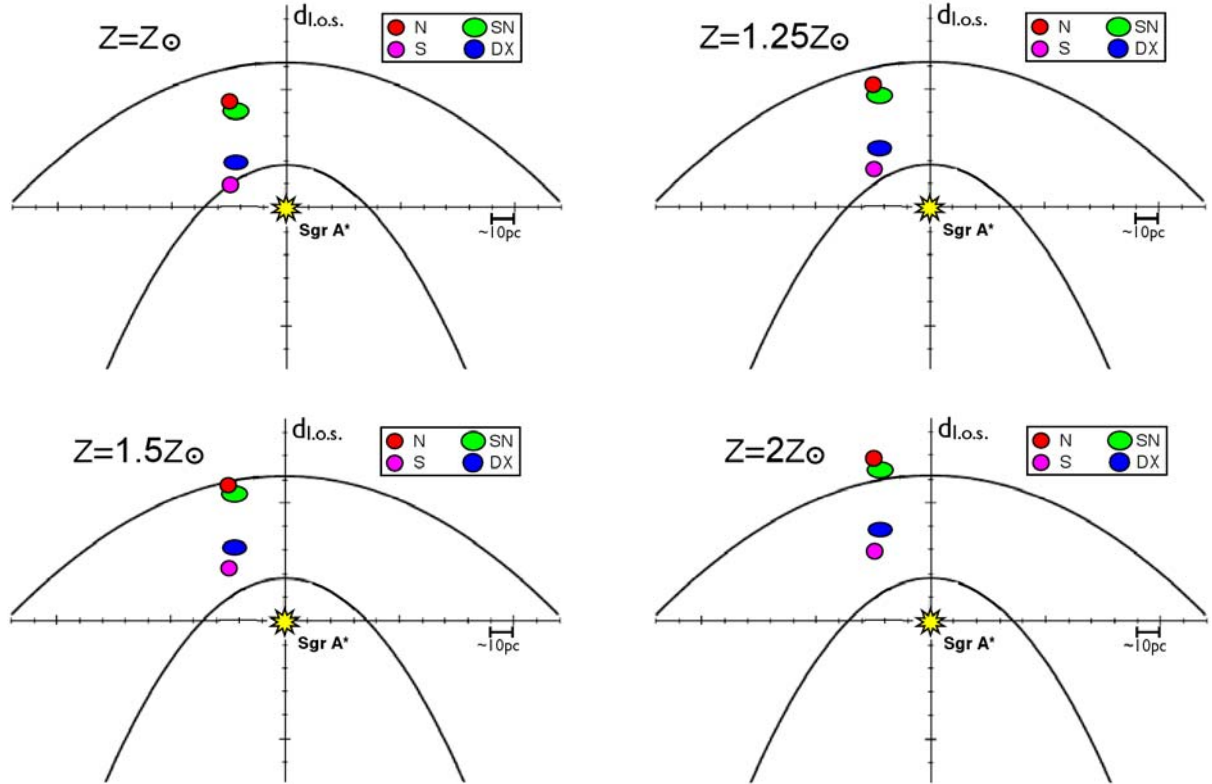


Fig. 6. The relative locations of the four MCs as inferred from the XRN/Sgr A* outburst model suggested by [Ponti et al. \(2010\)](#). This is the view of the Galactic plane as seen from above (i.e. the clouds positions are shown projected onto the plane). The two parabolas in each sketch represent curves of constant path length for a burst of ionizing flux propagating outwards from Sgr A*. The size of each cloud has been enlarged by a factor of 3.5 to aid the visualisation. The distance (in parsecs) along the line of sight (relative to Sgr A*) is plotted along the Y axis (see also [Table 5](#)). The SMBH Sgr A* is located at the origin of the axes and marked by a yellow star. The four panels represent the situation for an assumed metallicity of 1, 1.25, 1.5 and 2 times the solar value.

For $Z = 1.25$, the N, S and SN clouds all lie in the outburst region. In this case, and more generally for a metallicity range of 1.2–1.4 times solar, the XRN/Sgr A* outburst model can, in principle, explain the observed fluorescence both in terms of the observed line flux and the lack of strong variability. Within this framework, the separation of the N and S clouds is inferred to be between 30–40 pc which seems to be a highly unlikely scenario (as noted previously). However, given the uncertainty in measuring the optical depths of the individual clouds based on the available N_H measurements, it is at least plausible that this unlikely cloud separation is a consequence of the limited precision of the optical depth estimates.

An alternative to the Sgr A* outburst hypothesis is that the energising photons are supplied by other nearby sources; indeed the GC region hosts numerous X-ray transient sources ([Muno et al. 2005, 2006](#); [Porquet et al. 2005a,b](#)). We note that [Koyama et al. \(2003\)](#) have studied the diffuse Fe-K features from the MCs in the AC surroundings using *Chandra* which, through its sharp angular resolution, is better able to delineate the shape of the 6.4-keV bright regions. These authors first suggested that the line emission is probably due to sources other than a past intense flare on Sgr A*. Particularly for the N and S MCs, the different surface brightness of two different regions within the same MC (the -30 km s^{-1} MC, [Wang et al. 2006](#)) would need to be explained in terms of varying optical depths if the irradiation is from a single (relatively distant) bright source. Given the proximity of these clouds to the AC, the alternative scenario of bombardment by low-energy CR electrons certainly merits consideration (see below).

4.1.2. The peculiar case of the DX cloud

We now consider the DX cloud, which is *unique* amongst the GC MC that are 6.4-keV bright in that it has exhibited both an increase and decrease in its Fe- K_α flux. The variability measured in the DX MC is too fast to have been produced by the same Sgr A* flare which has been proposed to have illuminated the other XRN in the CMZ, since the inferred flare duration for the latter is greater than ten years. Notwithstanding this constraint, we have determined the location along line of sight of the DX cloud using the same method as employed above (see [Table 5](#) for the detailed results). As we can see in all the panels of [Fig. 6](#), the $d_{l.o.s}$ value for this cloud spans the range 20–40 pc, putting it squarely within the outburst region for any of the metallicity assumptions. Clearly, a simple XRN/Sgr A* picture as the one proposed by [Ponti et al. \(2010\)](#) is not consistent with our results on the DX cloud; on the other hand, we note that there is a source of potential errors introduced by the uncertain measurement of the distance along the line of sight. However, the fast variability measured for the Fe- K_α line flux points to an origin other than Sgr A*, whose flare luminosity is supposed to be constant over the whole flaring period. In this cloud, the non detection of the Fe-K edge is due to the poor statistics.

In the XRN hypothesis, the energising source could also be a transient source, most likely an X-ray binary (XRB) system. The typical 2–10 keV luminosities reached by these X-ray point sources are of the order of 10^{36} and 10^{38} erg/s for a high-mass and a low-mass system respectively. Assuming an XRB embedded in the DX cloud ($\Omega = 1$ in the formula above), the required

X-ray luminosity is $\sim 2 \times 10^{35}$ erg/s, compatible with a transient source hypothesis. On the other hand, if we consider the possibility that the primary source might have been a low-mass XRB lying in a region of high obscuration immediately behind the cloud, then it could be up to ~ 10 pc from the cloud assuming a typical X-ray luminosity of 10^{38} erg/s. Given the X-ray luminosity requirements, we favor the scenario where a high-mass XRB is located inside, or closely behind, the cloud. Among such systems, transients sources can have orbital periods of years, with a flare timescale of some months. Of course, given the very limited information we have to date, we cannot exclude the contributions of more than one X-ray source or even perhaps a more exotic contribution to the fluorescence excitation from a short-lived particle bombardment episode.

4.1.3. EW of the Fe- K_α line

The relatively high values of the line *EW* measured in the three MCs closest to the AC are readily explained in terms of photoionization of the clouds by X-ray photons. In the context of the XRN model, the *EW* of the Fe- K_α line is expected to be high (about 1 keV), since the direct source of photoionization is not seen by the observer (e.g., Sunyaev & Churazov 1998). Therefore, our results seem to confirm that some kind of X-ray reflection is working in the MCs close to the AC; however, the lack of a strong present-day X-ray source leaves open the discussion about the identity of the putative energizing source. Although the *EW* of the 6.4-keV line measured in the three MCs is about 1 keV, we notice that the error ranges (90% confidence level) are always consistent with an *EW* value of 0.6–0.7 keV; this is what expected from fluorescence to be induced by particle bombardment (subrelativistic electrons) in a MC with an Fe abundance of about twice the solar value. We therefore cannot exclude a priori one of the two ionization mechanisms only based on the present measurements of the *EW*.

4.1.4. Fe K absorption edge

We did not measure any Fe-K absorption edge at 7.1 keV; although the detection of such a spectral feature is challenging for N_H values of the clouds in the range 10^{22} – 10^{23} cm $^{-2}$, we notice that in other GC clouds with similar density an Fe-K edge has been measured (Ponti et al. 2010). We could only find upper limits to the optical depth of the absorption edge, listed in Table 4.

4.1.5. Spectral hardness

The shape of the non-thermal continuum associated with the production of the 6.4-keV line can also, in principle, provide a clue as to the nature of the excitation mechanism. Our analysis suggests that this non-thermal continuum has a very hard spectrum with a power-law photon index $\Gamma = 1.0^{+0.1}_{-0.2}$. In the particle bombardment scenario, $\Gamma = 1.3$ – 1.4 is expected for CR electron spectra typical of the GC region (e.g. Yusef-Zadeh et al. 2002a), although a somewhat harder spectrum might be indicative of an unusual particle environment in the vicinity of the AC. Therefore, the hardness of the power law component might be best explained in terms of the bombardment of the clouds by cosmic ray particles emanating from the AC itself. Of course, the pure reflection scenario also predicts a reflected X-ray continuum significantly harder than that characteristic of the illuminating X-ray source (Revnivtsev et al. 2004; Terrier et al. 2010).

4.2. The CR particle bombardment hypothesis

An alternative explanation of the Fe fluorescence involves the interaction of CR particles (electrons and/or protons) with cold molecular matter. In this context the cross-section for collisional ionization of Fe has its highest value in the energy range extending from the energy of the Fe-K edge (at 7.1 keV) up to a few MeV. Recently, two main ideas have been developed in order to explain the Fe fluorescent emission, namely bombardment by either electrons (Yusef-Zadeh et al. 2007a) or protons (Dogiel et al. 2009). Valinia et al. (2000) first suggested that a distribution of low-energy CR electrons (LECRE) might be responsible for the Galactic Ridge X-ray emission. In their model, the hard X-ray continuum associated with the Ridge is produced by non-thermal bremsstrahlung as the LECRe interact with the material of the ISM. The low-ionization line emission from Fe and other metals is similarly produced through LECRe collisions with the neutral medium. The energies of the LECRe involved in this mechanism span the range 7.1 keV to ~ 100 keV. In this setting, the flux of the 6.4-keV line is directly proportional to the density of the target material (in our case the MCs), and the in situ kinetic energy density of the LECRe, while the resulting *EW* of the Fe- K_α line spans the range 0.3–0.7 keV for metallicities from solar to twice the solar value.

The 6.4-keV photon production rate inferred from the results of Valinia et al. (2000) is

$$F_{6.4} = \frac{4.8 \times 10^{-22} H}{4\pi D^2} \left(\frac{U}{\text{eV/cm}^3} \right) \text{ photons/cm}^2/\text{s},$$

where $F_{6.4}$ is the 6.4-keV line flux in units of photons/cm 2 /s, D is the distance to the emitting cloud (8 kpc for the GC clouds), U is the kinetic energy density of LECRe (in eV/cm 3) and H is the number of H atoms in the MC (see fourth column of Table 2).

Using the estimates of the number of H atoms given in Table 2, we have calculated the LECRe energy density required to explain the observed 6.4-keV fluxes (Table 3). We find that the energy density required in the N, S and SN knots is 61, 216 and 77 eV/cm 3 . For the DX cloud, assuming the Fe-line flux to be 1.6×10^{-6} photons/cm 2 /s (i.e. the minimum in the lightcurve), the required energy density is 32 eV/cm 3 . All these four values have to be divided by two in case the Fe abundance we assume is twice the solar value (as discussed above). For comparison, Valinia et al. (2000) found that the mean LECRe energy density required to explain the Galactic Ridge was 0.2 eV/cm 3 ; moreover, using the same model, Yusef-Zadeh et al. (2002a) found that the Fe- K_α line flux measured from the G0.13-0.13 MC requires a LECRe energy density of 150 eV/cm 3 , a value very similar to what found for the AC MCs.

A significant enhancement of the CR flux in the GC region compared to the Galactic plane is perhaps to be expected. Also energetic particles might well be accelerated in the shocked stellar winds which characterise the core region of the AC (White 1985; Yusef-Zadeh et al. 2003), potentially resulting in a greatly enhanced energy density in the vicinity of the cluster. The fact that the 6.4-keV line flux measured from region S is significantly higher than that from knot N could be a consequence of the stellar distribution within the cluster. As shown first by Yusef-Zadeh et al. (2002b) and later by Law & Yusef-Zadeh (2004), the southern component of the cluster is populated by strong stellar-wind sources, which are also detectable at radio wavelengths (Lang et al. 2001). These massive early-type stars could also be present in binary systems, and be the origin of the X-ray flaring activity

recently discovered by Capelli et al. (2011). Massive interacting binaries are efficient in producing X-ray emission in the shock fronts within the winds and also in accelerating CRs.

In a variation on this theme, Wang et al. (2006) proposed the interaction of the -30 km s^{-1} MC with the AC to be the origin of the Fe fluorescent emission. These authors found that the -30 km s^{-1} molecular complex is moving towards the AC with a relative velocity of $\sim 120 \text{ km s}^{-1}$. In this picture, particles are accelerated in reversed shocks through efficient Fermi first order mechanism, and gain enough energy to be able to ionize Fe atoms within the cloud.

In the case of the DX cloud, we discovered the *fastest* variability ever found for a GC MC. Given that the timescale of the variability is comparable to the size of the cloud, this would seem to completely rule out bombardment by sub-relativistic particles as the origin of the increase in the Fe- $K\alpha$ line flux measured from this complex. However, it is at least plausible that the underlying base level of the 6.4-keV lightcurve could represent a relatively constant particle contribution to the fluorescence budget. The presence of high energy particles in this cloud may be inferred from radio continuum observations at 20 cm (see Fig. 1b in Yusef-Zadeh et al. 2002b) in which non-thermal filaments propagate westwards from the Radio Arc into the general region of this cloud.

The nature of the non-thermal radio filaments in the GC region is still under debate. The concentration of these strong radio features in the inner Galaxy may well be related to the peculiar high energy activity of this unique region (Yusef-Zadeh 2003). Many attempts have been made to explain the formation of such structures, involving all the likely high energy sources connected with the GC region, that is the SMBH Sgr A*, massive wind binaries, Galactic winds and gas clouds. A recent suggestion is that the origin of these filaments might be due to the presence of many young and massive stellar clusters in the central region of the Galaxy (Yusef-Zadeh 2003). Whatever the origin of the radio filaments, their presence in the region suggests that cloud fluorescence induced by particle bombardment must be present at some level (i.e. Fukuoka et al. 2009). Potentially, X-ray flaring events of the sort recently discovered in the AC (Capelli et al. 2011), might also induce some variability in the local LECRe energy density, which could in turn impart variability in the fluorescence signal, albeit delayed and smeared out relative to the activity in the primary source.

Recently, Dogiel et al. (2009) have suggested that at least some of the Fe- $K\alpha$ line emission from MCs in the CMZ can be produced by the interaction of high energy protons (with energies in the range of several hundred MeV) with the molecular target. This model naturally explains the presence of both the non-thermal components in the spectrum of the GC hard X-ray emission (Koyama et al. 2009). As in the LECRe model, this scenario has some difficulties in accounting for the rapid variability of the 6.4-keV line found in some MCs in the inner GC region, including the DX cloud.

LECRE with $E \sim 100 \text{ keV}$ can be stopped by matter with column densities of about $10^{22} \text{ H atoms/cm}^2$ (Tatischeff 2003). Considering the sizes and column densities of the MCs quoted in Table 2, we can calculate that LECRe lose their energy within depths that are at most half the cloud size. Similarly, Dogiel et al. (2009) estimate that high energy protons in the GC region typically travel for 0.1–0.3 pc before being stopped through interactions with the ISM. These estimates imply that particle-induced fluorescence and other interactions will occur only in the outer shell of a dense cloud. Both LECRe and high energy protons lose most of their energy in heating the ISM rather than

in producing non-thermal continuum emission or fluorescence photons. Yusef-Zadeh et al. (2007b) argue that the reason the temperature of the MCs in the CMZ is higher ($T \sim 100\text{--}200 \text{ K}$) than that measured for MCs in the Galactic plane (about 20 K) is due to CR particle heating. In fact, the ionization rates modelled for LECRe and high energy proton bombardment of MCs are in good agreement with the temperature enhancements which are actually measured (Yusef-Zadeh et al. 2002a; Dogiel et al. 2009). Furthermore, both Huettemeister et al. (1993) and Rodríguez-Fernández et al. (2001) measured temperature gradients in most of the MCs in the GC region; this is a natural consequence of the interaction of subrelativistic electrons and protons largely with the surface layers of the MCs.

5. Summary

In this paper we have used data from *XMM-Newton* to study the diffuse Fe- $K\alpha$ fluorescent line emission emanating from the region surrounding the AC. Our results can be summarized as follows:

- We detected four Fe- $K\alpha$ bright MCs in the vicinity of the AC. Two of these are new detections (referred to herein as knots SN and DX).
- The Fe- $K\alpha$ line flux measured from the three clouds nearest to the AC (knots N, S and SN) has remained constant over an interval of eight years. The *EW* of the 6.4-keV line in the spectra of these clouds is measured to be about 1 keV. This is consistent with the origin of the Fe fluorescence being the irradiation of the MCs by X-rays. The XRN/Sgr A* outburst scenario, which has been recently suggested as the explanation for all the Fe-K fluorescence seen in the GC region, in broad terms fits the observations, although with some reservations. Other X-ray sources, in particular nearby X-ray binaries and transients, might well have contributed to the 6.4 keV line production. Within the errors, the Fe- $K\alpha$ line *EW*s are also compatible with the CR bombardment scenario, with the AC itself being a likely location of the requisite particle acceleration. In this context, the required particle kinetic energy density is roughly a hundred times higher than that previously estimated as a possible explanation of the hard X-ray Galactic Ridge emission, but such an enhancement might well arise from in situ acceleration of particles in the AC. The particle candidates are subrelativistic electrons and/or protons.
- We have discovered variability on a timescale of a few years in the Fe- $K\alpha$ line emission from the DX cloud. Because of the highly variable emission, this is unlikely to be the product of past high-state activity in Sgr A*. We propose an X-ray binary to be the energising source of this fluorescence. Moreover, on the top of the variability, this molecular complex shows a non-zero underlying level of the fluorescent line flux, suggesting the possibility that both the reflection and CR bombardment processes may be working in tandem. The variability seen in the DX cloud is the *fastest* yet recorded in the GC region and, to date, it is the only example of a MC exhibiting both an increase and subsequent decrease in its Fe fluorescent emission.

The available data for the AC region does not allow the precise measurement of the spectral parameters relating to the Fe fluorescence phenomenon, namely the *EW* of the Fe $K\alpha$ line and the absorption edge at 7.1 keV. However, with deeper observations there is the prospect of fully characterising the emission

spectrum and dispelling any ambiguity concerning the underlying excitation process. This would be an important further step in the on-going investigation of whether Sgr A* has exhibited AGN-like activity in the recent past.

Acknowledgements. *XMM-Newton* is an ESA science mission with instruments and contributions directly funded by ESA Member States and the USA (NASA). R.C. thanks Prof. Dr. Y. Tanaka and Dr. Lara Sidoli for many useful discussions. R.C. also thanks Dr. Konrad Dennerl and Dr. Silvano Molendi for useful discussions about the *XMM-Newton* background subtraction and modelling.

References

- Abbey, T., Carpenter, J., Read, A., et al. 2006, in *The X-ray Universe 2005*, ed. A. Wilson, ESA Special Publication, 604, 943
- Amo-Baladrón, M. A., Martín-Pintado, J., Morris, M. R., Muno, M. P., & Rodríguez-Fernández, N. J. 2009, *ApJ*, 694, 943
- Baganoff, F. K., Bautz, M. W., Brandt, W. N., et al. 2001, *Nature*, 413, 45
- Capelli, R., Warwick, R. S., Cappelluti, N., et al. 2011, *A&A*, 525, L2
- De Luca, A., & Molendi, S. 2004, *A&A*, 419, 837
- Degenaar, N., & Wijnands, R. 2010, *A&A*, 524, A69
- Dogiel, V., Cheng, K., Chernyshov, D., et al. 2009, *PASJ*, 61, 901
- Fabian, A. C., Rees, M. J., Stella, L., & White, N. E. 1989, *MNRAS*, 238, 729
- Fukuoka, R., Koyama, K., Ryu, S. G., & Tsuru, T. G. 2009, *PASJ*, 61, 593
- Gillessen, S., Eisenhauer, F., Trippe, S., et al. 2009, *ApJ*, 692, 1075
- Handa, T., Sakano, M., Naito, S., Hiramatsu, M., & Tsuboi, M. 2006, *ApJ*, 636, 261
- Hickox, R. C., & Markevitch, M. 2007, *ApJ*, 671, 1523
- Huettemeister, S., Wilson, T. L., Bania, T. M., & Martín-Pintado, J. 1993, *A&A*, 280, 255
- Inui, T., Koyama, K., Matsumoto, H., & Tsuru, T. G. 2009, *PASJ*, 61, 241
- Koyama, K., Maeda, Y., Sonobe, T., et al. 1996, *PASJ*, 48, 249
- Koyama, K., Murakami, H., & Takagi, S. 2003, *Astron. Nachr. Supp.*, 324, 117
- Koyama, K., Hyodo, Y., Inui, T., et al. 2007, *PASJ*, 59, 245
- Koyama, K., Takikawa, Y., Hyodo, Y., et al. 2009, *PASJ*, 61, 255
- Lang, C. C., Goss, W. M., & Rodríguez, L. F. 2001, *ApJ*, 551, L143
- Law, C., & Yusef-Zadeh, F. 2004, *ApJ*, 611, 858
- Leccardi, A., & Molendi, S. 2008, *A&A*, 486, 359
- Morris, M., & Serabyn, E. 1996, *ARA&A*, 34, 645
- Morrison, R., & McCammon, D. 1983, *ApJ*, 270, 119
- Muno, M. P., Pfahl, E., Baganoff, F. K., et al. 2005, *ApJ*, 622, L113
- Muno, M. P., Bauer, F. E., Bandyopadhyay, R. M., & Wang, Q. D. 2006, *ApJS*, 165, 173
- Muno, M. P., Baganoff, F. K., Brandt, W. N., Park, S., & Morris, M. R. 2007, *ApJ*, 656, L69
- Murakami, H., Koyama, K., Sakano, M., Tsumimoto, M., & Maeda, Y. 2000, *ApJ*, 534, 283
- Nakajima, H., Tsuru, T. G., Nobukawa, M., et al. 2009, *PASJ*, 61, 233
- Nandra, K., George, I. M., Mushotzky, R. F., Turner, T. J., & Yaqoob, T. 1997, *ApJ*, 477, 602
- Nobukawa, M., Koyama, K., Tsuru, T. G., Ryu, S. G., & Tatischeff, V. 2010, *PASJ*, 62, 423
- Ponti, G., Terrier, R., Goldwurm, A., Belanger, G., & Trap, G. 2010, *ApJ*, 714, 732
- Porquet, D., Predehl, P., Aschenbach, B., et al. 2003, *A&A*, 407, L17
- Porquet, D., Grosso, N., Bélanger, G., et al. 2005a, *A&A*, 443, 571
- Porquet, D., Grosso, N., Burwitz, V., et al. 2005b, *A&A*, 430, L9
- Porquet, D., Grosso, N., Predehl, P., et al. 2008, *A&A*, 488, 549
- Predehl, P., Costantini, E., Hasinger, G., & Tanaka, Y. 2003, *Astron. Nachr.*, 324, 73
- Revnivtsev, M. G., Churazov, E. M., Sazonov, S. Y., et al. 2004, *A&A*, 425, L49
- Rodríguez-Fernández, N. J., Martín-Pintado, J., Fuente, A., et al. 2001, *A&A*, 365, 174
- Ryu, S. G., Koyama, K., Nobukawa, M., Fukuoka, R., & Tsuru, T. G. 2009, *PASJ*, 61, 751
- Smith, R. K., Brickhouse, N. S., Liedahl, D. A., & Raymond, J. C. 2001, *ApJ*, 556, L91
- Strüder, L., Briel, U., Dennerl, K., et al. 2001, *A&A*, 365, L18
- Sunyaev, R., & Churazov, E. 1998, *MNRAS*, 297, 1279
- Tanaka, Y. 2002, *A&A*, 382, 1052
- Tatischeff, V. 2003, in *EAS Publications Series*, ed. C. Motch, & J.-M. Hameury, 7, 79
- Terrier, R., Ponti, G., Bélanger, G., et al. 2010, *ApJ*, 719, 143
- Tsuboi, M., Handa, T., & Ukita, N. 1999, *ApJS*, 120, 1
- Tsumimoto, M., Hyodo, Y., & Koyama, K. 2007, *PASJ*, 59, 229
- Turner, M. J. L., Abbey, A., Arnaud, M., et al. 2001, *A&A*, 365, L27
- Valinia, A., Tatischeff, V., Arnaud, K., Ebisawa, K., & Ramaty, R. 2000, *ApJ*, 543, 733
- Wang, Q. D., Dong, H., & Lang, C. 2006, *MNRAS*, 371, 38
- White, R. L. 1985, *ApJ*, 289, 698
- Yusef-Zadeh, F. 2003, *ApJ*, 598, 325
- Yusef-Zadeh, F., Law, C., & Wardle, M. 2002a, *ApJ*, 568, L121
- Yusef-Zadeh, F., Law, C., Wardle, M., et al. 2002b, *ApJ*, 570, 665
- Yusef-Zadeh, F., Nord, M., Wardle, M., et al. 2003, *ApJ*, 590, L103
- Yusef-Zadeh, F., Muno, M., Wardle, M., & Lis, D. C. 2007a, *ApJ*, 656, 847
- Yusef-Zadeh, F., Wardle, M., & Roy, S. 2007b, *ApJ*, 665, L123